Near-field optical experiments on low-symmetry split-ring-resonator arrays

Daniela Diessel,[1,2,*] Manuel Decker,[1,2] Stefan Linden,[1,2,3] and Martin Wegener[1,2]

[1]*Institut für Nanotechnologie, Karlsruhe Institute of Technology (KIT), Hermann-von-Helmholtz-Platz 1, D-76344 Eggenstein-Leopoldshafen, Germany*

[2]*Institut für Angewandte Physik and DFG-Center for Functional Nanostructures (CFN), Karlsruhe Institute of Technology (KIT), Wolfgang-Gaede-Strasse 1, D-76131 Karlsruhe, Germany*

[3]*Physikalisches Institut, Universität Bonn, Nußallee 12, 53115 Bonn, Germany*

**Corresponding author: daniela.diessel@kit.edu*

Received July 6, 2010; accepted September 16, 2010;
posted October 11, 2010 (Doc. ID 131247); published October 27, 2010

Effective symmetric and antisymmetric eigenmodes of coupled plasmonic resonances play a crucial role in many photonic metamaterials. Recently, we discussed a particular arrangement of metallic split-ring resonators that is planar, hence enabling direct experimental access to the different eigenmodes via near-field optical microscopy. In this Letter, corresponding optical experiments are presented and compared with simple theoretical modeling, providing a direct confirmation of our previous, more indirect conclusions. © 2010 Optical Society of America

OCIS codes: 160.3918, 180.4243.

Coupling effects play a major role in photonic metamaterials. For example, coupling enables the antisymmetric current mode in cut-wire pairs (a common "meta-atom" used, e.g., in the fishnet structure) that leads to artificial magnetism at optical frequencies [1,2]. Furthermore, coupling also occurs between the different meta-atoms for vertical stacking as well as for planar meta-atom arrangements [3–7]. For two coupled resonances, the resulting effective modes are simply symmetric and antisymmetric, respectively. Numerical simulations to visualize them have been published numerous times. However, it would still be desirable to visualize the modes by direct experiments. For normal split-ring-resonator (SRR) arrays, such experimental results have been published [8]. In this Letter, using a recently introduced low-symmetry planar arrangement of gold SRRs leading to effective "ferromagnetic" and "antiferromagnetic" modes [4,5] and employing scanning near-field optical microscopy, we directly visualize the difference between the two modes experimentally.

Figure 1 illustrates our experimental setup. We use far-field illumination of the photonic metamaterial samples from the glass substrate side under normal incidence of light. Precisely, we focus 1 mW of power from a cw semiconductor laser diode to a spot of roughly 50 μm in diameter using a 50 cm focal length lens. The incident polarization is linear and can be varied by rotating a Glan–Thompson polarizer. A scanning near-field optical microscope (SNOM) aperture tip collects the light on the other side of the sample. This SNOM tip has been fabricated by an HF etching procedure [9], followed by high-vacuum evaporation of 250 nm Al, and focused-ion-beam milling to open an aperture of about 180 nm in diameter. The light emerging from the other end of the optical fiber is sent to a Peltier-cooled InGaAs photodiode. The signals are normalized to the signal obtained when locating the SNOM tip beside the SRR arrays, i.e., over the bare glass substrate. Note that, in principle, the resulting normalized signals can locally exceed unity. Spatial images are obtained by scanning the tip in close proximity to the sample in the constant-distance mode [10] while recording the detector signal.

Electron micrographs of the low-symmetry SRR samples used in our experiments are shown in Fig. 2(a), and the corresponding far-field optical transmittance spectra are shown in Fig. 2(b). In essence [4], the two eigenmodes of such arrays can be excited by the two diagonal linear polarizations. The frequency splitting of the transmittance minima is a direct result of the SRR interactions in the array [4]. For the low-frequency or long-wavelength antisymmetric or "antiferromagnetic" mode, the magnetic dipole-moments of adjacent SRRs are antiparallel at any instant in time; for the high-frequency or short-wavelength symmetric or "ferromagnetic" mode, they are parallel. Ideally, one would like to detect the magnetic field component normal to the array plane in a phase-resolved manner [11]. However, this is not necessary here, as one expects the other electromagnetic field components of the two eigenmodes to also exhibit rather differing spatial distributions. Thus, we use a normal aperture-type SNOM tip, as shown in Fig. 1.

Corresponding measured SNOM images are shown in Figs. 2(c) and 2(d). Obviously, the SNOM images for the two different diagonal linear polarizations are distinctly different. For the polarization associated with the

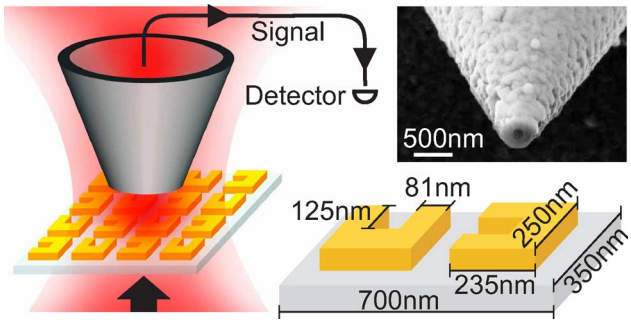

Fig. 1. (Color online) Illustration of our experimental setup of SNOM on low-symmetry SRR arrays. One primitive unit cell of the array (dimensions as indicated) is shown on the right-hand side. The gold thickness is 60 nm. The SEM image shows a typical aluminum-coated fiber probe.

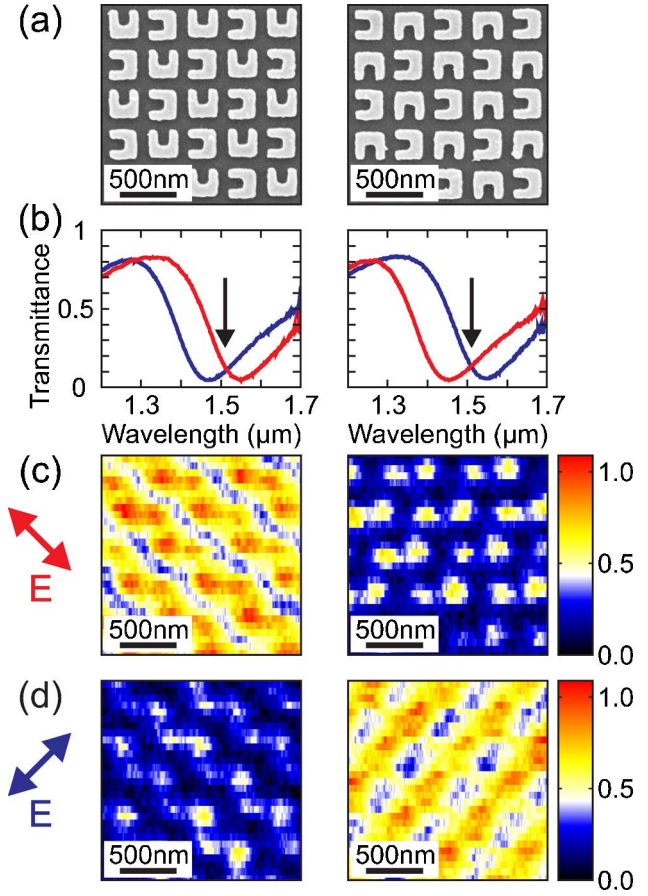

Fig. 2. (Color online) Summary of experimental results. The two columns correspond to two different gold SRR arrays on a glass substrate. (a) Electron micrographs, (b) measured normal-incidence far-field intensity transmittance spectra. (c), (d) SNOM images for a wavelength of 1510 nm [see arrows in (b)]. The respective incident diagonal linear polarizations are illustrated by the double arrows on the left-hand side.

antisymmetric eigenmode, we obtain bright diagonal bands, whereas we observe more separated and much dimmer spots for the orthogonal diagonal linear polarization. Importantly, the two images are expected to be identical without any SRR interactions. Thus, the observed differences provide a direct spatial visualization of SRR interaction effects. However, caution has to be exerted as such differences could, in principle, also arise from either unintentional asymmetries of the SNOM aperture or by unintentional asymmetries of the fabricated metamaterial samples. To rule out both artifacts, we have conducted various control experiments. One of them is shown in the right-hand side column of Fig. 2. Here, we have used a different SRR array on the same glass substrate that is a rotated version of the one on the left-hand side. Obviously, we find perfectly consistent results. Furthermore (not depicted), we have also physically rotated the same two SRR arrays (while keeping the SNOM tip fixed), again leading to perfectly consistent results.

To further test our interpretation, we compare our experimental results with theoretical modeling. Here, we follow our recent approach [12] that has been successful in the context of negative-index double-fishnet-type photonic metamaterials. We start from numerical calculations of the local electromagnetic fields using the commercial software CST Microwave Studio, which is based on a finite-integration technique. The sample geometry is taken from the measured electron micrographs [see Fig. 2(a)] and is depicted in Fig. 3(a). The gold SRR thickness is taken as 60 nm. As usual, the metal is described by the free-electron Drude model with plasma frequency $\omega_{\mathrm{pl}} = 1.37 \times 10^{16}\ \mathrm{s}^{-1}$ and the collision frequency $\omega_{\mathrm{col}} = 1.4 \times 10^{14}\ \mathrm{s}^{-1}$. The refractive index of the glass substrate is taken as $n = 1.5$. Corresponding far-field transmittance spectra are shown in Fig. 3(b). They excellently agree with the experiment in Fig. 2(b). To compute the SNOM images, we have extended our previous purely heuristic approach [12].

A circularly symmetric SNOM aperture equally transmits the two orthogonal polarization directions. Each consists of two contributions from the fields 20 nm above the sample: (i) the parallel electric field component, averaged over the aperture (a circle with a radius of 140 nm) and (ii) the difference between opposite points on the aperture edge of the electric field component perpendicular to the aperture plane, projected onto the respective direction. Phenomenologically, contribution (ii) is multiplied with a factor of 0.66, and a phase lag of 0.17π is added to contribution (i). The two complex contributions (i) and (ii) are added for each polarization component. The SNOM signal results as the sum of the modulus squared of the two components. For further details, see the Supporting Information of our previous

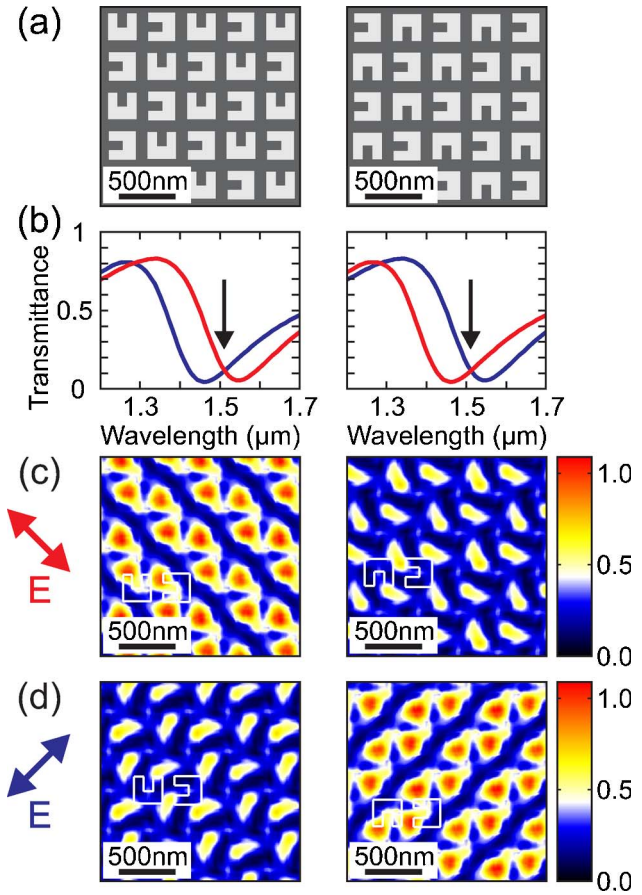

Fig. 3. (Color online) Results from numerical calculations presented in the same manner as the experiments shown in Fig. 2.

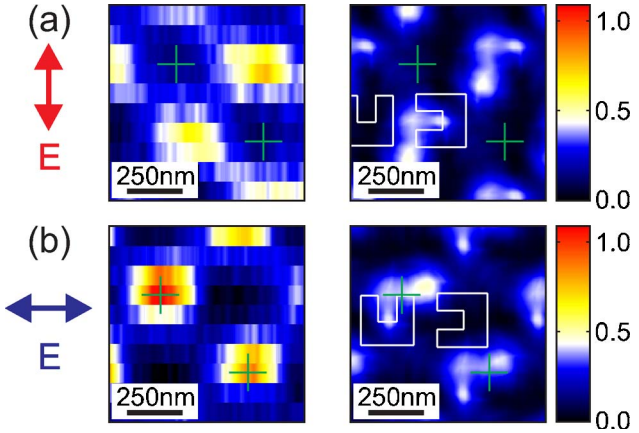

Fig. 4. (Color online) Results of measurements (left-hand side) and simulations (right-hand side) for (a) vertical and (b) horizontal linear polarization at a wavelength of 1510 nm. As a visual guide, in all four images the same two positions are marked (green). Additionally, the location of the SRR unit cell in the simulations is shown in white.

work [12]. The phase lag added here slightly differs from [12]. This is not surprising considering that the SNOM probes used here and in [12] have rather different geometries. In particular, the opening angle is 55° here, whereas it has been 18° in our previous work.

The resulting simulated SNOM images are shown in Figs. 3(c) and 3(d)—represented exactly as the experiments in Fig. 2. Obviously, the overall qualitative agreement is very good. We again obtain bright diagonal bands from the "antisymmetric" mode, whereas we observe more separated and dimmer spots for the "symmetric" mode. Note that the spatial average of the near-field images in Figs. 3(c) and 3(d) is not directly connected to the far-field transmittance in Fig. 3(b), which is nearly identical for the two diagonal linear polarizations. This aspect results from the fact that the near-field signal is a complicated sum of different contributions (see above).

Finally, in Fig. 4 we present experiments and simulations at a wavelength of 1510 nm for horizontal and vertical (rather than diagonal) incident linear polarization—both of which are not eigenpolarizations [4]. Whereas diagonal incident polarization results in one spot per SRR, we now observe only one for every two SRRs (left-hand side of Fig. 4), again in good agreement with the calculations (right-hand side). Simulations and experiments at other wavelengths in the range from 1430 to 1610 nm show a closely similar behavior (not displayed). For the wavelength of 1510 nm, we have exemplified that when the incident polarization is rotated by 90°, the brightest and darkest spots switch positions.

In conclusion, by using scanning near-field optical microscopy, we have directly visualized the effects of in-plane interactions of low-symmetry SRR arrays. Numerical calculations nicely agree with the experiment.

We acknowledge support by the Deutsche Forschungsgemeinschaft (DFG) and the State of Baden-Württemberg through the DFG-Center for Functional Nanostructures (CFN) within subproject A 1.5. The project PHOME acknowledges the financial support of the Future and Emerging Technologies (FET) programme within the Seventh Framework Programme for Research of the European Commission, under FET–Open grant 213390. The project METAMAT is supported by the Bundesministerium für Bildung und Forschung. The research of S. L. is further supported through a Helmholtz-Hochschul-Nachwuchsgruppe (VH-NG-232). The Ph.D. education of D. D. and M. D. is embedded in the Karlsruhe School of Optics & Photonics (KSOP).

References

1. G. Dolling, C. Enkrich, M. Wegener, J. F. Zhou, C. M. Soukoulis, and S. Linden, Opt. Lett. **30**, 3198 (2005).
2. V. M. Shalaev, W. Cai, U. K. Chettiar, H.-K. Yuan, A. K. Sarychev, V. P. Drachev, and A. V. Kildishev, Opt. Lett. **30**, 3356 (2005).
3. N. Liu, H. Guo, L. Fu, S. Kaiser, H. Schweizer, and H. Giessen, Nat. Mater. **7**, 31 (2008).
4. M. Decker, S. Linden, and M. Wegener, Opt. Lett. **34**, 1579 (2009).
5. M. Decker, S. Burger, S. Linden, and M. Wegener, Phys. Rev. B **80**, 193102 (2009).
6. L. Solymar and E. Shamonina, *Waves in Metamaterials* (Oxford U. Press, 2009).
7. I. Sersic, M. Frimmer, E. Verhagen, and A. F. Koenderink, Phys. Rev. Lett. **103**, 213902 (2009).
8. T. Zentgraf, J. Dorfmüller, C. Rockstuhl, C. Etrich, R. Vogelgesang, K. Kern, T. Pertsch, F. Lederer, and H. Giessen, Opt. Lett. **33**, 848 (2008).
9. S. Mononobe and M. Ohtsu, J. Lightwave Technol. **14**, 2231 (1996).
10. K. Karrai and R. D. Grober, Appl. Phys. Lett. **66**, 1842 (1995).
11. M. Burresi, D. van Oosten, T. Kampfrath, H. Schoenmaker, R. Heideman, A. Leinse, and L. Kuipers, Science **326**, 550 (2009).
12. M. Burresi, D. Diessel, D. van Oosten, S. Linden, M. Wegener, and L. Kuipers, Nano Lett. **10**, 2480 (2010).